ACS APPLIED MATERIALS & INTERFACES

Research Article

www.acsami.org

Mesoporous Titanium Zirconium Oxide Nanospheres with Potential for Drug Delivery Applications

Xiaojian Wang,[†] Dehong Chen,[‡] Lu Cao,[‡] Yuncang Li,[§] Ben J. Boyd,[⊥] and Rachel A. Caruso*[,†,‡]

[†]CSIRO Materials Science and Engineering, Private Bag 33, Clayton South, Victoria 3169, Australia

[‡]Particulate Fluids Processing Centre, School of Chemistry, The University of Melbourne, Melbourne, Victoria 3010, Australia

[§]Institute for Frontier Materials, Deakin University, Geelong, Victoria 3217, Australia

[⊥]Drug Delivery, Disposition and Dynamics, Monash Institute of Pharmaceutical Sciences, Monash University (Parkville Campus), 381 Royal Pde, Parkville, Victoria 3052, Australia

Supporting Information

ABSTRACT: Mesoporous titanium zirconium (TiZr) oxide nanospheres with variable Ti to Zr ratios were synthesized using sol–gel chemistry followed by solvothermal treatment. These oxide nanospheres exhibited similar diameters (~360 nm), high surface areas (from 237 ± 2 to 419 ± 4 $m^2 g^{-1}$), and uniform pore diameters (~3.7 nm). Three drugs, ibuprofen, dexamethasone, and erythromycin, were loaded into the TiZr oxide nanospheres. The TiZr oxide nanospheres exhibited a high loading capacity, up to 719 mg g^{-1}, and sustained release profiles in phosphate buffered saline (PBS) at pH 7.4. The mesoporous TiZr oxide nanospheres also exhibited hydrolytic stability, as evidenced by the retention of the integrity of the mesostructures after drug release in PBS for 21 days.

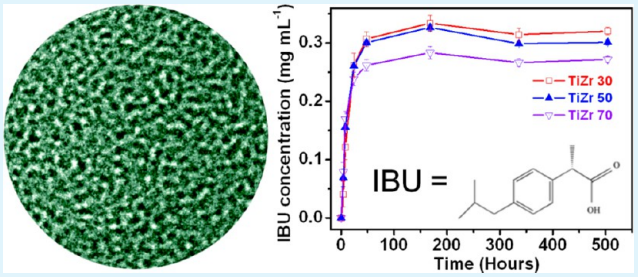

KEYWORDS: *porous materials, templating, drug delivery, titanium oxide, zirconium oxide, nanomaterials*

INTRODUCTION

Nanotechnology for drug delivery has attracted much attention in recent years.[1−7] The application of nanotechnology makes it possible to achieve (a) improved delivery of poorly water-soluble drugs; (b) stimuli-responsive delivery of drugs in a cell- or tissue-specific manner; (c) codelivery of two or more drugs, therapeutic modality for combination therapy; and (d) drug delivery, diagnosis, and multiple therapies in one platform.[7] Recent breakthroughs on inorganic nanosized delivery vehicles, such as mesoporous silica nanoparticles (MSNs), have brought new possibilities to this research field.[6] MSNs have several attractive features, including high surface area, tunable pore size, controllable particle size and shape, and dual-functional exterior and interior surfaces, for application as a novel drug delivery system. Mesoporous silica materials, such as MCM-41 or SBA-15, have been reported to have a high drug (ibuprofen) loading capacity of 23 to 33 wt % and sustained drug release profiles.[8−10] By designing MSNs as hollow core/mesoporous shell structures, the amount of drug molecule encapsulated can be increased to more than 1 g drug per gram MSNs.[11] Because of structural stability, the size- and shape controllable mesostructure can store pharmaceutical drugs and prevent their degradation and premature release before reaching target. Mesoporous materials that are stable under physiological conditions are also desired as platforms for biosensing,[12] cell imaging,[13] and encapsulating therapeutic agents.[14−16]

Bioceramics, such as zirconium oxide, are biocompatible and have a history of being used as biomaterials in dentistry and as components in total hip implants.[17−19] Recently nanostructured titanium and zirconium oxide were shown to be bioactive, which is evidenced by surface formation of an apatite layer when immersed in a simulated body fluid (SBF).[20,21] It indicates that titanium and zirconium oxide may be good candidates for drug delivery vehicles or for multifunctional coatings on metallic implants.[22,23] In this study, we present the synthesis of mesoporous titanium zirconium (TiZr) mixed oxide nanospheres which could be used as potential local drug delivery systems for treating bone-related diseases. Hence, three drugs were chosen for this study: Ibuprofen (IBU) was chosen as a model drug as it is relatively insoluble in water, but is readily solubilized in common organic solvents. IBU is frequently employed as a model drug for assessing controlled delivery because of its molecular size of about 1.0 × 0.5 nm.[8] Dexamethasone (DEX) was selected as a target drug, as it has been used for treating rheumatoid arthritis by virtue of its anti-inflammatory function.[24] Erythromycin (ERY), a macrolide antibiotic, was also selected, as it is commonly used in bone cement for controlling infections.[25]

The addition of Zr^{4+} during the synthesis of titanium oxide produces a Zr–O–Ti network, which gives an amorphous mixed TiZr metal oxide. The high surface area mesoporous TiZr oxide nanospheres with variable Ti to Zr ratios were

Received: July 30, 2013
Accepted: October 3, 2013
Published: October 22, 2013

synthesized by using sol–gel chemistry using hexadecylamine as a structure-directing agent.[26] These oxide nanospheres exhibited similar diameters (~360 nm), high surface areas (from 237 ± 2 to 419 ± 4 m^2 g^{-1}), and uniform pore diameters (~3.7 nm). These spheres were loaded with the drugs, and the release profile was analyzed. Using IBU as an example, the drug loading capacity was shown to depend on the surface area, achieving 719 mg g^{-1} IBU loading for the TiZr oxide nanospheres with a Ti:Zr mole ratio of 7:3. Beside the different drug loading capacities, all the IBU-loaded TiZr oxide spheres showed a sustained release profile. The mesoporous TiZr oxide nanospheres also exhibited hydrolytic stability under physiological conditions, as evidenced by the retention of the integrity of the mesostructures after drug release in phosphate buffered saline (PBS) for 21 days. The mesoporous TiZr oxide nanospheres reported in the present work share common features with MSNs, that is, large surface area and high drug loading capacity. In comparison with MSNs, the TiZr oxide spheres exhibited hydrolytic stability. The mesoporous TiZr oxide spheres could be promising stable bioplatforms for delivering drugs and other biological agents.

EXPERIMENTAL SECTION

Materials. Titanium(IV) isopropoxide (97%), zirconium(IV) propoxide (70% in propanol), and hexadecylamine (HDA, 90%) were purchased from Sigma–Aldrich. Absolute ethanol (>99.7% Merck), potassium chloride (AR, BDH), and deionized water (Milli-Q, 18.2 MΩ cm) were used for nanosphere synthesis. Ibuprofen (98% Sigma), dexamethasone (>97% Sigma), erythromycin (98% Sigma), *n*-hexane (98% Merck), 10× concentrated phosphate buffered saline (Sigma-Aldrich, diluted before application), and hydrochloric acid (37% Sigma-Aldrich) were used for the drug loading and release studies. A human osteosarcoma cell line with osteoblastic properties, (SaOS2, which was obtained from Barwon Biomedical Research, Victoria, Australia), were used in the present study. Other cell culture chemicals include: minimum essential media (MEM) (Gibco), 1% nonessential amino acid (Sigma-Aldrich), 10% fetal bovine serum (Bovogen), 10,000 units mL^{-1} penicillin-10,000 μg mL^{-1} streptomycin (Gibco), 0.1% Trypsin-5 mM EDTA (Sigma-Aldrich), 0.4% amphostat B (In Vitro Technologies), 2% paraformaldehyde (Sigma-Aldrich), Triton-X100 (Promega), 1% phalloidin (Sigma-Aldrich), and 4′-6-diamidino-2-phenylindole (Sigma-Aldrich).

Preparation of TiZr Oxide Nanospheres. The TiZr (Ti to Zr atomic ratios of 7:3 (TiZr30), 5:5 (TiZr50), and 3:7 (TiZr70)) oxide precursor nanospheres were prepared via a sol–gel process using HDA as a structure-directing agent.[26] In a typical synthesis (TiZr30), 7.95 g of HDA was dissolved in 790 mL of ethanol, and then added to a 5.44 mL of Milli-Q H_2O and 3.20 mL of 0.1 M KCl solution. A premixture of 7.96 mL of zirconium propoxide, 12.89 mL of titanium isopropoxide, and 10 mL of ethanol was added to the above solution under vigorous stirring. A white suspension was obtained and kept static for 18 h. The spheres were centrifuged and washed with ethanol three times and dried in air at room temperature. After that, 1.6 g of the resulting precursor nanospheres were dispersed into a mixture of 20 mL of ethanol and 10 mL of Milli-Q water and underwent a solvothermal treatment at 160 °C for 16 h. Such solvothermally treated nanospheres were collected by filtration, washed with ethanol three times, and dried in air. Finally the dried powder was calcined at 500 °C for 2 h in air to remove the organic components.

Characterization. Morphology and particle size of the products were observed using a scanning electron microscope (SEM, FEI QUANTA 200F) operated at 15 kV under low vacuum mode. A FEI Tecnai F20 transmission electron microscope was used to record the TEM images and selected area electron diffraction (SAED) patterns of the resulting TiZr oxide nanospheres. Specific surface area and porosity of the products were measured at −196 °C using a Micromeritics Tristar 3020 analyzer according to a standard procedure reported previously.[26] Particle size and zeta potential were measured on a Brookhaven 90 Plus particle size analyzer. A powder X-ray diffractometer (Bruker D8) was used to investigate the crystal phase of the products. A FT-IR spectrometer (PE IR Spectrum ASCII PEDS 1.60) was employed to obtain the FT-IR spectra. Materials were ground, mixed with KBr and pressed into pellets for testing. The OH density of the TiZr oxide nanospheres was determined using a thermogravimetric method (on a Mettler Toledo TGA/SDTA851e instrument) following literature.[27]

Drug Loading and Release. A 1.00 g portion of the TiZr oxide nanospheres was added to a 50 mL drug–hexane solution (2, 5, 10, 30 g L^{-1}) in a flask. The flask was immediately covered to prevent solvent from evaporating. The dispersion of TiZr oxide nanospheres was done by ultrasound and the flask oscillated (160 rpm) at 37 °C for 21 days. The drug-loaded TiZr oxide was separated by centrifugation. After being washed three times with hexane, drug-loaded TiZr oxide spheres were dried under vacuum at 60 °C. The amount of drug loaded into the TiZr oxide nanospheres was calculated according to the concentration of drug remaining in the supernatant, against a calibration curve (n = 3).

For the release studies, the drug-loaded TiZr oxide samples were dispersed in 100 mL of PBS (pH 7.4) at 37 °C, shaking at a rate of 100 rpm. Aliquots (2 mL) of the drug-release medium were collected for UV–vis (Cary 300) analysis at specific wavelengths (264 nm for IBU, 238 nm for DEX, and 236 nm for ERY) at given time intervals and replaced with the same volume of fresh PBS. Calculation of the corrected concentration of released drug was based on the following equation:

$$C_{tcorr} = C_t + \frac{v}{V}\sum^{t-1} C_t$$

Where C_t is the apparent concentration at time t, C_{tcorr} is the corrected concentration at time t, V is the total volume of dissolution medium, and v is the volume of sample taken. The drug-release media (at 4 h, 48 h, 7 days, and 21 days) were submitted to ICP-AES (Varian 730 Axial Simultaneous ICP-AES system) for the detection of any released Ti and Zr ions.

In Vitro Biocompatibility Assessment. One milligram of TiZr30 oxide nanospheres was washed in Milli-Q water and sterilized prior to cell culture experiments, which were performed in 24 well non-treated tissue culture plates. The dry powder was dispersed into a 10 mL culture medium by ultrasound. SaOS2 cells were cultured at 37 °C in a humidified atmosphere of 5% CO_2/air. Minimum essential media (MEM) supplemented with 1% nonessential amino acid, 10% fetal bovine serum, 10,000 units mL^{-1} penicillin-10,000 μg mL^{-1} streptomycin and 0.4% amphostat B were used as cell culture media. SaOS2 cells were seeded into the TiZr oxide containing solution and negative controls at a density of 10,000 cells per well. After 3 days, cells were harvested with 0.1% Trypsin-5 mM EDTA. Cell counts were obtained by the trypan blue exclusion method, whereby dead cells are stained blue and live cells remain clear. The cell viability was determined by the ratio of live cells to the total number of cells per sample.[28,29] Details can be found in the literature.[29] The cell morphology of SaOS2 cultured with TiZr oxide nanospheres and the control sample were observed by confocal microscopy (Leica SP5).

RESULTS AND DISCUSSION

A sol–gel self-assembly process was employed for the synthesis of the mesoporous oxide nanospheres using hexadecylamine (HDA) as a structure forming agent. In this process, zirconium propoxide (ZrP) and titanium isopropoxide (TIP) were added to an ethanol and water mixture containing HDA to produce the TiZr oxide nanospheres. By changing the ratio of TIP to ZrP, the composition of the final material was controlled to give $Ti_{0.7}Zr_{0.3}O_2$ (TiZr30), $Ti_{0.5}Zr_{0.5}O_2$ (TiZr50), and $Ti_{0.3}Zr_{0.7}O_2$ (TiZr70). Adding Zr (IV) during the sol–gel synthesis of a Ti oxide can produce mesoporous TiZr mixed oxides, which remain amorphous and have higher surface area after moderate calcination (500 °C) than the crystalline mesoporous individual oxides of

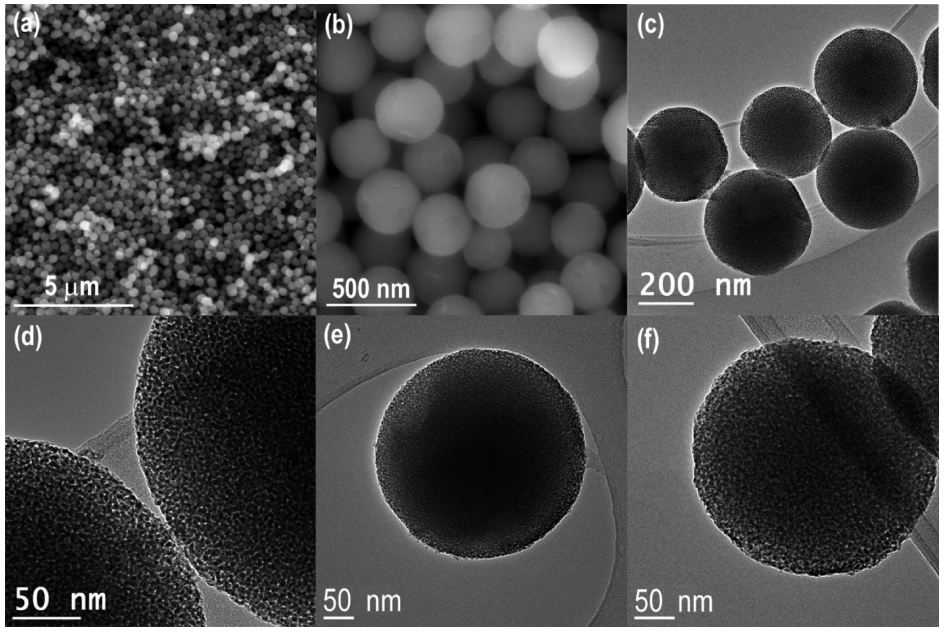

Figure 1. SEM images (a, b) and TEM images (c, d) of the mesoporous TiZr30 nanospheres, TEM image of the mesoporous TiZr50 (e) and TiZr70 (f) nanospheres. SEM images were obtained without metal sputter coating.

TiO_2 or ZrO_2 (Supporting Information, Tables S1, S2).[26,30,31] These TiZr oxide nanospheres with high surface area and enhanced thermal stability have been applied to preliminary testing as a bioplatform that could have drug delivery function. Electron microscopy images of the mesoporous TiZr oxide nanospheres are shown in Figure 1. These particles were spherical in shape with an average diameter of ~360 nm (see Table 1). As the diameter of the spheres was primarily affected by the amount of water added during sol–gel synthesis, the difference in the diameter of the three TiZr oxide nanosphere samples was small. Transmission electron microscopy (TEM) images (Figure 1c–f) show that all the TiZr oxide nanospheres possess "wormhole-like" pore structures, which were uniformly observed throughout the whole sphere, indicating three-dimensional (3D) interconnected mesoporous networks. All the TiZr oxide samples were amorphous, as observed in the selected area electron diffraction (SAED) patterns (see Supporting Information, Figure S1a as an example), and also supported by the wide-angle XRD patterns (Supporting Information, Figure S1b). The amorphous structure was retained even after calcination at 500 °C, allowing retention of the mesostructure in the calcined product.

Table 1. Physical Properties of the Calcined Mesoporous TiZr Oxide Nanospheres of Varied Compositions

sample name	TiZr30	TiZr50	TiZr70
S_{BET} (m^2 g^{-1})	419 ± 4	289 ± 3	237 ± 2
pore diameter (nm)	3.6	3.8	3.8
pore volume (cm^3 g^{-1})	0.50	0.34	0.26
particle diameter (nm)	360 ± 40	370 ± 40	360 ± 40
OH density (# /nm^2)	3.0	3.1	3.1
OH molar density (mmol g^{-1})	1.58	1.48	1.20

The nitrogen sorption isotherms of the TiZr oxide spheres are shown in Figure 2. The isotherms can be classified as Type IV isothermal curves,[32] which are commonly observed in mesostructured materials. The Brunauer–Emmett–Teller (BET) surface area (S_{BET}) of the TiZr30 spheres was measured to be 419 ± 4 m^2 g^{-1} and the Barrett–Joyner–Halenda pore diameter and pore volume were 3.6 nm and 0.50 cm^3 g^{-1}, respectively. With increasing Zr content the surface area and pore volume decreased (Table 1). It has been shown that the presence of Zr (IV) can retard the crystallization of TiO_2; with sufficient Zr

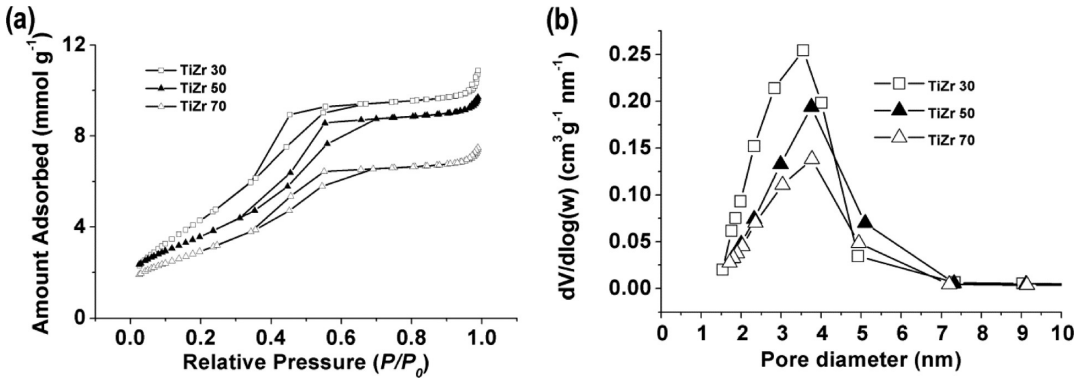

Figure 2. Nitrogen sorption isotherms (a) and pore size distribution (b) of the mesoporous TiZr oxide nanospheres of varied compositions.

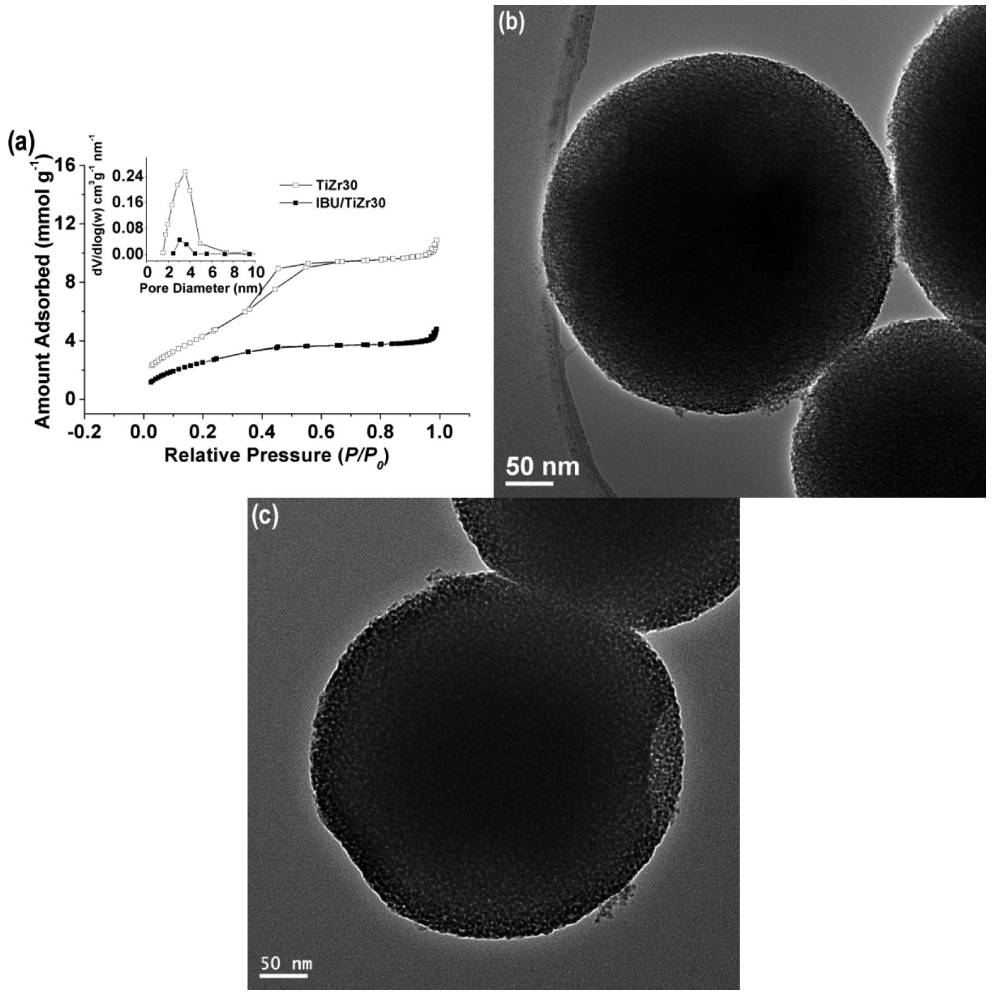

Figure 3. Nitrogen sorption isotherms and pore size distribution (a) of the mesoporous TiZr30 nanospheres before and after loading in 30 mg mL^{-1} IBU, TEM image of the IBU-loaded TiZr30 nanospheres (b), and TEM image of the IBU/TiZr30 nanospheres (c) after release in PBS for 21 days.

(IV) (Zr:Ti atomic ratio >0.2) crystallization to the anatase titania phase can be completely inhibited at temperatures at which the anatase phase generally becomes apparent.[26] The phase transition inhibiting effect may be related to the substitution of Ti^{4+} ions by the Zr^{4+}.[33] As a result, the formation of Zr−O−Ti bonds can inhibit the mobility of the Ti atoms in the inorganic framework, which is required to initiate the phase transition. In addition, the incorporation of Zr (IV) into the mesoporous network changed the surface properties of the metal oxide spheres. The isoelectric point (IEP) of TiZr30 was determined to be 5.1, which is between that of pure TiO_2 (anatase 6.2)[34] and ZrO_2 (3.4).[14] The IEP decreased to 5.0 and 4.9 for TiZr50 and TiZr70, respectively (Supporting Information, Figure S2).

To explore the potential of these TiZr oxide nanospheres as drug carriers, three drugs commonly used to treat bone-related complications, namely, ibuprofen (IBU), dexamethasone (DEX), and erythromycin (ERY), have been chosen as model drugs. After infiltrating drugs into the mesoporous TiZr oxide nanospheres, a significant decrease in surface area and pore volume was observed as compared with that of the bare TiZr oxide nanospheres, indicating that the mesopores within the TiZr oxide nanospheres were filled or blocked by the drug molecules. Taking the IBU-loaded TiZr30 sample as an example, the gas sorption hysteresis associated with mesopores disappeared, and the pore volume (seen as the peak in the pore size distribution curve) obviously decreased (Figure 3).

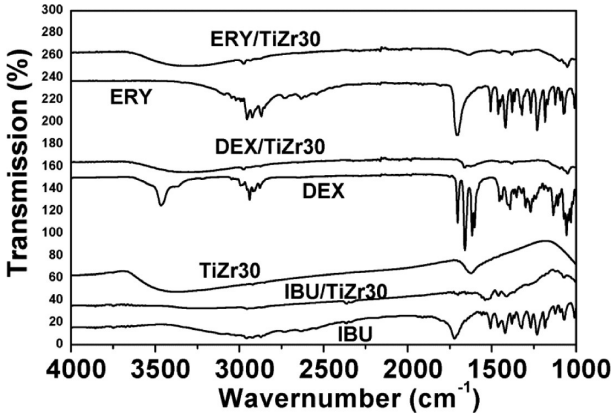

Figure 4. FT-IR spectra of the pure IBU, DEX, ERY, the mesoporous TiZr30 nanospheres, and the drug-loaded TiZr30 nanospheres.

The S_{BET} and pore volume decreased from 419 to 219 m^2 g^{-1}, and from 0.50 to 0.12 cm^3 g^{-1}, respectively. The drug loading capacity of the TiZr oxide nanospheres increased with the drug concentration in solution (Table 2). From a solution containing 30 mg mL^{-1} IBU, 719 mg IBU was loaded into 1 g of the TiZr30, higher than that of TiZr50 (688 mg g^{-1}) and TiZr70 (682 mg g^{-1}). This trend in loading capacity for the materials

Table 2. Drug Loading Capacities of the Mesoporous TiZr Oxide Nanospheres for the Drugs IBU, DEX, and ERY

	TiZr30 loading capacity (mg g^{-1})	TiZr50 loading capacity (mg g^{-1})	TiZr70 loading capacity (mg g^{-1})
2 mg mL^{-1} IBU	70 ± 14	68 ± 15	63 ± 13
5 mg mL^{-1} IBU	154 ± 25	147 ± 16	145 ± 17
10 mg mL^{-1} IBU	285 ± 28	274 ± 34	265 ± 27
30 mg mL^{-1} IBU	719 ± 165	689 ± 129	682 ± 146
2 mg mL^{-1} DEX	49 ± 15	38 ± 16	40 ± 12
2 mg mL^{-1} ERY	37 ± 11	29 ± 8	17 ± 6

was observed at other drug concentrations, as shown in Table 2.

Fourier transform infrared (FT-IR) spectra confirmed the presence of drug within the nanospheres (see Figure 4). For the IBU loading, the detection of a band centered around 1710 cm^{-1} due to the C═O stretching (H-bonded) vibration, as well as the C−C (aromatic) stretching (~1512 cm^{-1}) and CH_3 antisymmetric deformation (~1465 cm^{-1}), indicates the incorporation of IBU into the TiZr oxide nanospheres. Similarly, the corresponding bands of DEX and ERY were evident for the drug-loaded samples, Figure 4. From TEM observations, see an example in Figure 3b, there were no large drug crystals observed on the sphere surfaces or between the spheres. It was assumed from the TEM analysis, FT-IR, and gas sorption data that the drugs were adsorbed on the walls of the mesopores, or partially blocked the mesopores.

To evaluate the release profile of the drug-loaded TiZr oxide nanospheres (IBU/TiZr, DEX/TiZr, and ERY/TiZr), the drug-loaded samples were dispersed in phosphate buffered saline (PBS) solutions (pH 7.4). All three drug-loaded TiZr oxide

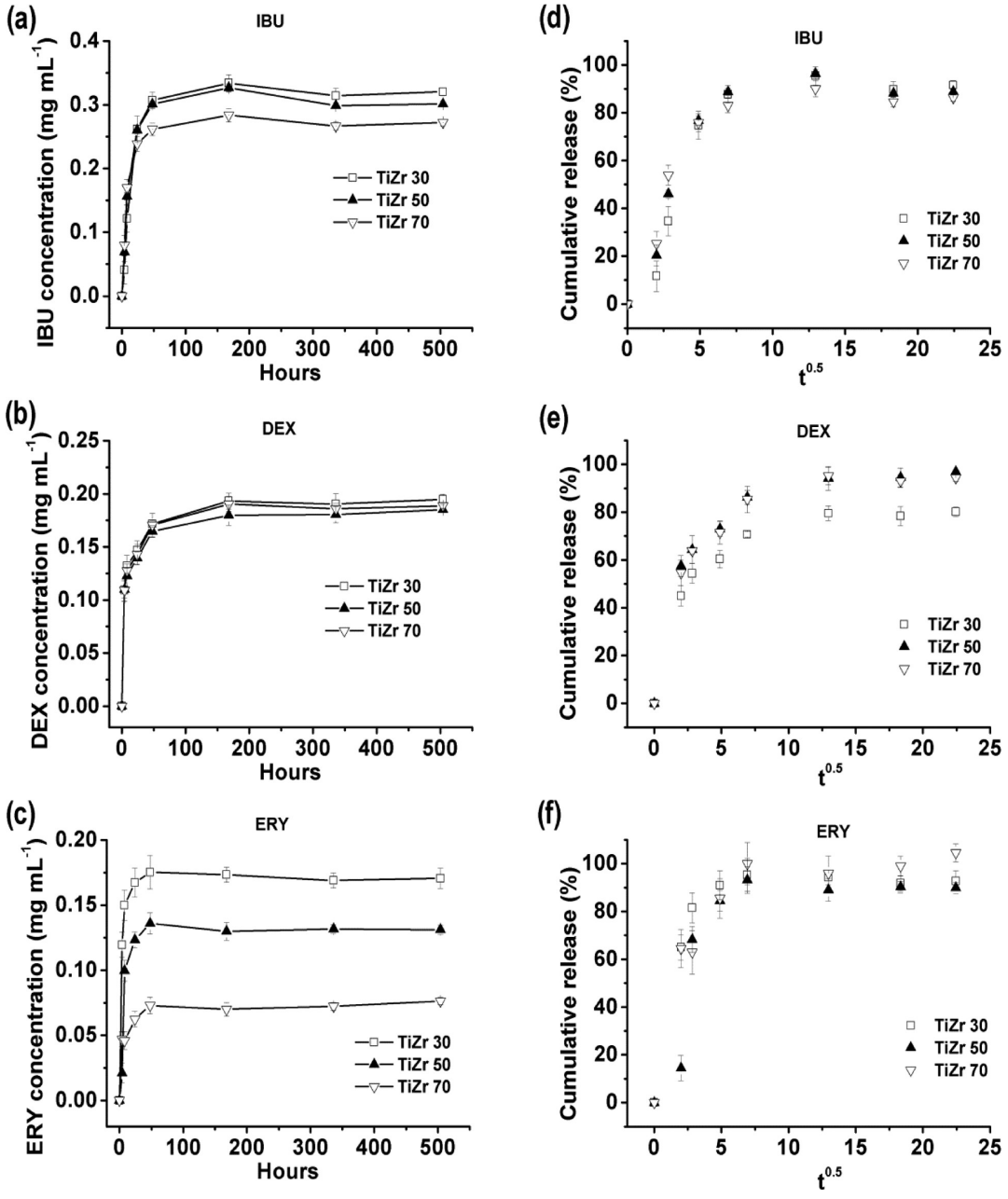

Figure 5. Release kinetics (a−c) of IBU, DEX, and ERY from the mesoporous TiZr30, TiZr50, and TiZr70 oxide nanospheres in pH 7.4 PBS over 21 days. Cumulative drug release percentage as a function of the square root of time (hour) for the drug-loaded TiZr oxide nanospheres (d−f) in pH 7.4 PBS.

systems showed sustained release with a relatively fast release in the initial stages (24 h). The drug release reached a plateau after which the drug concentration remained constant (from 48 h) in PBS, Figure 5. Drug molecules entrapped in mesoporous materials are extremely mobile at ambient temperature.[35] Only weak interactions exist between the drug and the matrix, and the initial release is directed by a diffusion process. The kinetics of release from the TiZr spheres can be described using the Higuchi model ($C = K{\cdot}t^{1/2}$),[8] where C is the cumulative amount of released drug, $t^{1/2}$ is the square root of time, and K is a constant. The drug release from the TiZr oxides shows a linear relationship between the cumulative amount of released drug and the square root of time (0–48 h), Figure 5, indicating a diffusion process. However, the drug-loaded systems displayed a two-step release profile composed of an initial burst followed by a slow release in PBS, which is commonly observed in other types of inorganic drug delivery systems, such as MCM-41 and SBA-15.[9,10] The release of all the three drugs occurs primarily in the first 4 days. This kind of profile can be useful when an immediate high dose is required, for example, for acute infections or inflammations. It is expected that greater control over both drug loading and release could be achieved by surface functionalization, which could be conducted on the mesoporous TiZr oxides as they showed a high density of hydroxyl groups on the surface (Table 1). It is expected that a prolonged drug release profile could be obtained after surface functionalization, as demonstrated on mesoporous SiO_2 and templated bioglass drug delivery vehicles.[36,37] Further research is needed to find out the drug load and release profiles of surface functionalized TiZr oxide.

One of the advantages of using inorganic mesoporous materials as drug carriers is that their structures can be quite stable in biological environments and hence they are not prone to premature degradation, and they have the potential to provide good deliveries at the target site. To test the hydrolytic stability of mesoporous TiZr oxide nanospheres, aliquots of the IBU-release medium were collected over the period of drug release to determine the concentrations of Ti (IV) and Zr (IV) ions by using inductively coupled plasma atomic emission spectroscopy (ICP-AES). No Ti (IV) or Zr (IV) ions could be detected in any of these media, which suggests that the TiZr oxide nanospheres were stable in pH 7.4 PBS. The mesostructure of the oxide nanospheres after drug release in PBS for 21 days was also investigated by TEM (shown in Figure 3c). No observable change was found in the mesoporous structure after drug release, indicating hydrolytic stability of the mesoporous TiZr oxide nanospheres.

In addition to the stability, cyto-biocompatibility is also another important consideration when developing a drug carrier. To investigate the cyto-biocompatibility of the TiZr oxide nanospheres, human SaOS2 osteoblast-like cells were cultured for 3 days on the tissue culture plate (control) and in the presence of 100 mg L^{-1} to 500 mg L^{-1} TiZr oxide nanospheres (Figure 6). The cultured SaOS2 showed typical cubic shape, less elongated than fibroblasts in the presence of 100 mg L^{-1} TiZr30. After 3 days in culture, the cell viability (Figure 6c) was calculated by analyzing the number of live cells and dead cells using a live/dead assay. Cell viabilities of 92%, 92%, and 94% were achieved in the presence of the 100 mg L^{-1} TiZr30, TiZr50, and TiZr70 oxide nanospheres (Figure 6c). These cell viabilities are comparable to that (94%) of the control. The cytotoxicity of TiZr oxide nanospheres increased with the increasing concentration of the oxide spheres, which is

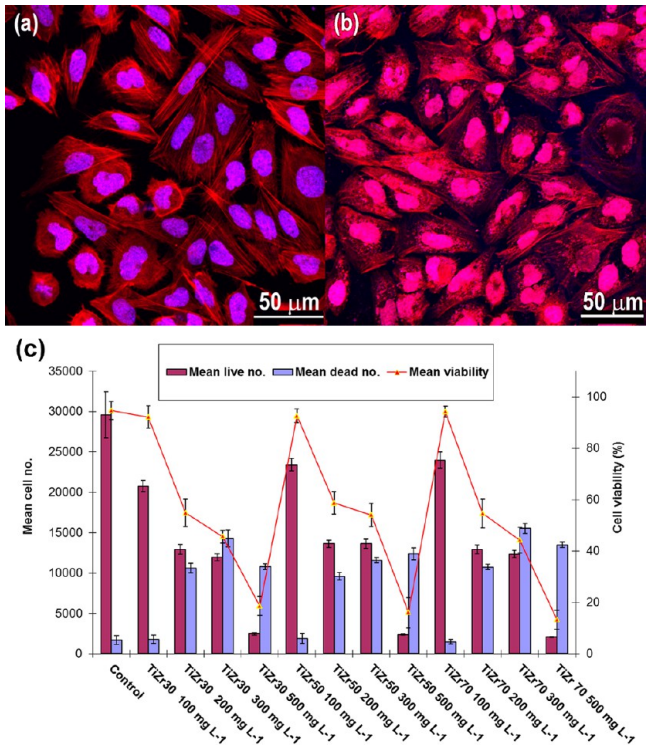

Figure 6. Confocal images of SaOS2 osteoblast-like cells on tissue culture plate (control, a) and in the presence of 100 mg L^{-1} TiZr30 oxide nanospheres (b) after culturing for 3 days. Cell number (c), and viability of the SaOS2 osteoblast-like cells after culturing for 3 days on the tissue culture plate (control) and in the presence of 100–500 mg L^{-1} TiZr30, TiZr50, and TiZr70 oxide nanospheres.

consistent with the observation of other nanoparticles, such as SiO_2 and TiO_2 nanoparticles.[38,39] When the concentration of the TiZr oxide spheres increased to 200 and 300 mg L^{-1}, the cell viability decreased to 55 and 46% for TiZr30. A further increase of concentration to 500 mg L^{-1} resulted in a cell viability of 19%. Similar trends were observed for both TiZr50 and TiZr70 spheres. The half maximal inhibitory concentration (IC50) was determined to be 250 mg L^{-1} for TiZr30, TiZr50, and TiZr70.

CONCLUSIONS

In summary, mesoporous TiZr oxide nanospheres with a diameter of ~360 nm, high surface area (up to 419 m^2 g^{-1}), and uniform mesopore size (~3.7 nm) have been synthesized using a facile sol–gel and solvothermal process. The applicability of these TiZr oxide nanospheres as potential drug delivery carriers was evaluated. Three drugs including IBU, DEX, and ERY for treating bone-related diseases have been loaded into the TiZr oxide nanospheres. Sustained release profiles were observed for these drug-loaded systems in PBS at pH 7.4. Moreover, the drug-loaded TiZr oxide nanospheres showed hydrolytic stability in PBS for 21 days and did not exhibit degradation under physiological conditions. Such a delivery system could potentially be applied as a local drug delivery agent for the treatment of bone-related complications.

ASSOCIATED CONTENT

Supporting Information

Selected area electron diffraction pattern and XRD pattern of TiZr30 oxide spheres, zeta potentials of the mesoporous TiZr

oxide nanospheres, physical properties of mesoporous TiO_2, ZrO_2 and 780 nm TiZr oxide spheres. This material is available free of charge via the Internet at http://pubs.acs.org.

AUTHOR INFORMATION

Corresponding Author

*E-mail: rcaruso@unimelb.edu.au.

Author Contributions

The manuscript was written through contributions of all authors.

Notes

The authors declare no competing financial interest.

ACKNOWLEDGMENTS

This research was financially supported by CSIRO through the OCE Science Leader Scheme and the Australian Research Council through the Discovery Project Scheme (DP0985744). R.A.C. and B.J.B. acknowledge the Australian Research Council for Future Fellowships (FT0990583 and FT120100697, respectively). The Advanced Microscopy Facility at The University of Melbourne is acknowledged for electron microscopy access.

REFERENCES

(1) Allen, T. M.; Cullis, P. R. *Science* **2004**, *303*, 1818−1822.
(2) Arcos, D.; Lopez-Noriega, A.; Ruiz-Hernandez, E.; Terasaki, O.; Vallet-Regi, M. *Chem. Mater.* **2009**, *21*, 1000−1009.
(3) Colilla, M.; Manzano, M.; Izquierdo-Barba, I.; Vallet-Regi, M.; Boissiere, C.; Sanchez, C. *Chem. Mater.* **2010**, *22*, 1821−1830.
(4) Palazzo, B.; Iafisco, M.; Laforgia, M.; Margiotta, N.; Natile, G.; Bianchi, C. L.; Walsh, D.; Mann, S.; Roveri, N. *Adv. Funct. Mater.* **2007**, *17*, 2180−2188.
(5) Sokolsky-Papkov, M.; Agashi, K.; Olaye, A.; Shakesheff, K.; Domb, A. J. *Adv. Drug Delivery Rev.* **2007**, *59*, 187−206.
(6) Arruebo, M. *Wiley Interdiscip. Rev. Nanomed. Nanobiotechnol.* **2012**, *4*, 16−30.
(7) Farokhzad, O. C.; Langer, R. *ACS Nano* **2009**, *3*, 16−20.
(8) Andersson, J.; Rosenholm, J.; Areva, S.; Lindn, M. *Chem. Mater.* **2004**, *16*, 4160−4167.
(9) Bass, J. D.; Grosso, D.; Boissiere, C.; Belamie, E.; Coradin, T.; Sanchez, C. *Chem. Mater.* **2007**, *19*, 4349−4356.
(10) He, Q.; Shi, J.; Zhu, M.; Chen, Y.; Chen, F. *Microporous Mesoporous Mater.* **2010**, *131*, 314−320.
(11) Chen, Y.; Chen, H.; Guo, L.; He, Q.; Chen, F.; Zhou, J.; Feng, J.; Shi, J. *ACS Nano* **2009**, *4*, 529−539.
(12) Zhang, Y.; Liu, S.; Sun, X. *Biosens. Bioelectron.* **2011**, *26*, 3876−3880.
(13) Fang, Y.; Gu, D.; Zou, Y.; Wu, Z.; Li, F.; Che, R.; Deng, Y.; Tu, B.; Zhao, D. *Angew. Chem. Int. Ed.* **2010**, *49*, 7987−7991.
(14) Tang, S.; Huang, X.; Chen, X.; Zheng, N. *Adv. Funct. Mater.* **2010**, *20*, 2442−2447.
(15) Yang, X.; Liu, X.; Liu, Z.; Pu, F.; Ren, J.; Qu, X. *Adv. Mater.* **2012**, *24*, 2890−2895.
(16) Zhou, L.; Li, Z.; Liu, Z.; Ren, J.; Qu, X. *Langmuir* **2013**, *29*, 6396−6403.
(17) Hench, L. L. *J. Am. Ceram. Soc.* **1991**, *74*, 1487−1510.
(18) Scarano, A.; Di Carlo, F.; Quaranta, M.; Piattelli, A. *J. Oral Implantol.* **2003**, *29*, 8−12.
(19) Guess, P. C.; Att, W.; Strub, J. R. *Clin. Implant Dent. Relat. Res.* **2012**, *14*, 633−645.
(20) Han, Y.; Yan, Y.; Lu, C.; Zhang, Y.; Xu, K. *J. Biomed. Mater. Res. A* **2009**, *88*, 117−127.
(21) Guo, L.; Zhao, J.; Wang, X.; Xu, X.; Liu, H.; Li, Y. *Int. J. Appl. Ceram. Technol.* **2009**, *6*, 636−641.
(22) Bjursten, L. M.; Rasmusson, L.; Oh, S.; Smith, G. C.; Brammer, K. S.; Jin, S. *J. Biomed. Mater. Res. A* **2010**, *92*, 1218−1224.
(23) McMaster, W. A.; Wang, X.; Caruso, R. A. *ACS Appl. Mater. Interfaces* **2012**, *4*, 4717−4725.
(24) Simmons, A.; Padsalgikar, A. D.; Ferris, L. M.; Poole-Warren, L. A. *Biomaterials* **2008**, *29*, 2987−2995.
(25) Wininger, David; Robert, F. *Antimicrob. Agents Chemother.* **1996**, *40*, 2675−2679.
(26) Chen, D. H.; Cao, L.; Hanley, T. L.; Caruso, R. A. *Adv. Funct. Mater.* **2012**, *22*, 1966−1971.
(27) Mueller, R.; Kammler, H. K.; Wegner, K.; Pratsinis, S. E. *Langmuir* **2003**, *19*, 160−165.
(28) Phillips, H. J. In *Tissue culture, methods and application*; Kruse, P. F., Patterson, M. K., Eds.; Academic Press: New York, 1973; p 406.
(29) Li, Y.; Wong, C.; Xiong, J.; Hodgson, P.; Wen, C. *J. Dent. Res.* **2010**, *89*, 493−497.
(30) Drisko, G. L.; Luca, V.; Sizgek, E.; Scales, N.; Caruso, R. A. *Langmuir* **2009**, *25*, 5286−5293.
(31) Kimling, M. C.; Caruso, R. A. *J. Mater. Chem.* **2012**, *22*, 4073−4082.
(32) Sing, K. S. W.; Everett, D. H.; Haul, R. A. W.; Moscou, L.; Pierotti, R. A.; Rouquerol, J.; Siemieniewska, T. *Pure Appl. Chem.* **1985**, *57*, 603−619.
(33) Schiller, R.; Weiss, C. K.; Landfester, K. *Nanotechnology* **2010**, *21*, 405603.
(34) Suttiponparnit, K.; Jiang, J.; Sahu, M.; Suvachittanont, S.; Charinpanitkul, T.; Biswas, P. *Nanoscale Res. Lett.* **2011**, *6*, 27.
(35) Azais, T.; Tourne-Peteilh, C.; Aussenac, F.; Baccile, N.; Coelho, C.; Devoisselle, J.-M.; Babonneau, F. *Chem. Mater.* **2006**, *18*, 6382−6390.
(36) Manzano, M.; Vallet-Regi, M. *J. Mater. Chem.* **2010**, *20*, 5593−5604.
(37) Balas, F.; Manzano, M.; Horcajada, P.; Vallet-Regi, M. *J. Am. Chem. Soc.* **2006**, *128*, 8116−8117.
(38) Jin, Y.; Kannan, S.; Wu, M.; Zhao, J. X. *Chem. Res. Toxicol.* **2007**, *20*, 1126−1133.
(39) Brayner, R. *Nano Today* **2008**, *3*, 48−55.